

## **PLASTIC BEHAVIOR OF NANO-SCALE SILICON STRUCTURE AT INTERMEDIATE TEMPERATURES**

Yoshitada Isono<sup>1</sup>, Takahiro Namazu<sup>2</sup> and Takeshi Tanaka<sup>1</sup>

<sup>1</sup> Department of Mechanical Engineering, Faculty of Science and Engineering,  
Ritsumeikan University, 1-1-1 Nojihigashi, Kusatsu-si, Shiga 525-8577, JAPAN

<sup>2</sup> Graduate Student, Department of Mechanical Engineering, Faculty of Science and Engineering,  
Ritsumeikan University, 1-1-1 Nojihigashi, Kusatsu-si, Shiga 525-8577, JAPAN

### **ABSTRACT**

This paper focuses on revealing specimen size and temperature effects on plasticity of nano-scale self-supported single crystal silicon (Si) beams for the design of electronic and micro electro-mechanical system (MEMS) devices. Four kinds of Si beams with widths from 200 to 800 nm and a thickness of 255 nm were fabricated on an Si diaphragm by means of field-enhanced anodization using AFM and anisotropic wet etching. Mechanical properties of the Si beams were evaluated by AFM bending testing at intermediate temperatures ranging from 295 K to 573 K in high vacuum. Young's modulus of the nano-scale Si showed temperature dependency but had no size effect, which was similar trend in Si bulk. The bending strength of the 200 nm-wide beams ranged from 15.87 to 17.76 GPa, which were approximately 1.5 times larger than the strength of the 800 nm-wide beams. Critical resolved shear stress and plastic strain range also exhibited specimen size and temperature dependency. The plastic strain range obviously increased with a reduction of the specimen size and an increase of temperature. This research showed that the plastic flow was easily induced in smaller sized Si beams on a nano-scale even if test temperature was 373 K, which was close to room temperature. AFM observations suggested that the slip line density would have determined the plastic strain range of nano-scale Si at intermediate temperatures.

### **KEYWORDS**

Single Crystal Silicon, AFM, Young's Modulus, Bending Strength, Plastic Strain Range, Slip Line

### **INTRODUCTION**

The evaluation of mechanical properties of nano-scale Si beams at intermediate temperatures is very important for the design of high-density electronic and MEMS devices, since the devices are serviced at room and intermediate temperatures, which may induce thermal stress. This stress can produce plastic deformation based on a dislocation of the  $1/2 \langle 110 \rangle \{111\}$  slip system that prohibits the electric conduction in Si. So far, mechanical properties of Si have just been estimated on a micro and millimeter scale at room temperature because of difficulties in problems associated with measuring ultra-small physical phenomena in an experiment at elevated temperatures [1], [2]. Few mechanical characterizations of micro/nano-scaled Si specimens at high temperature have also been performed. Frühauf, J. et al [3] carried out a plastic deformation process of micro-scale Si elements at 700 K – 1000 K for reshaping of the elements, however they did not propose any design criteria for Si because their work was not aimed at mechanical characterization. For safe and reliable designs of high-density electronic components, nano-scale material testing of Si at elevated temperatures is essential.

The objective of this research is to reveal the specimen size and temperature effects on Young's modulus and bending strength of nano-scale Si beams at intermediate temperatures ranging from 295 K to 573 K. Bending tests for the Si beams were carried out using AFM and the fracture probability was discussed using Weibull plots. The specimen size and temperature dependency of the plastic deformation behavior were also discussed in the light of observations of the slip line using the AFM.

**EXPERIMENTAL PROCEDURE**

**Fabrication of Nano-scale Si beam**

The field-enhanced anodization with an AFM was carried out for making Si fixed beams on a nanometer scale. Field-enhanced anodization is a method to draw a silicon dioxide (SiO<sub>2</sub>) film line with a width of less than 1 μm on an Si surface [4], which is used as the high precision mask pattern for the anisotropic wet etching with a solution of 20 % tetra-methyl ammonium hydroxide (TMAH). It was then possible to fabricate a nanometer scale Si structure after the etching. Figure 1 shows the field-enhanced anodization process with AFM. In this research, the SiO<sub>2</sub> film was anodized on a SIMOX wafer at the bias voltage of 20 V and at the scanning speed of 0.4 m/s, whereat the thickness of SiO<sub>2</sub> reached about 5 nm that was a sufficient film thickness for the TMAH wet etching.

Four kinds of Si beams were prepared in AFM bending tests. The Si beams with widths of 200, 300, 550 and 800 nm were fabricated by the wet etching with TMAH after the field-enhanced anodization. Figure 2 depicts a SEM photograph of nano-scale Si beams. The beams are oriented along the [110] direction in the (001) plane. The cross-section of the beam is a trapezoid owing to the anisotropic wet etching process. The nominal dimensions of the beams are listed in Table 1. The width, length and thickness values for each of the beams were measured by the AFM prior to the bending test. Si beams within ±5 % error of the dimensions listed in Table 1 have been used in the bending tests.

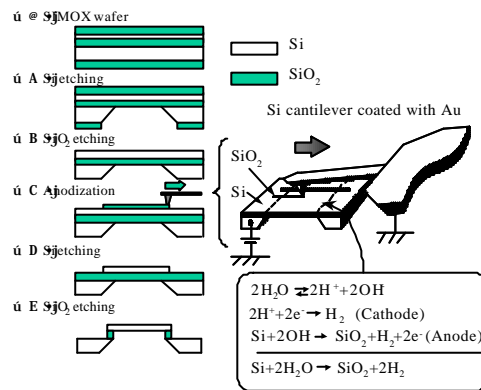


**Figure 1:** Fabrication process of nano-scale Si beam using field-enhanced anodization with AFM

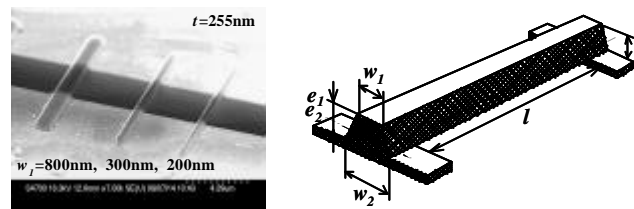


**Figure 2:** SEM photograph of Si beams along with a schematic of a beam

**Table 1**  
Nominal dimensions of nano-scale Si beams

Upper width $W_1$ [nm]	Lower width $W_2$ [nm]	Thickness $t$ [nm]	Length $l$ [mm]
200	370	255	6
300	470	255	6
550	720	255	6
800	980	255	6

### Test Procedure

Figure 3 illustrates a schematic diagram of the bending test using the AFM. A diamond tip with a tip radius of 100 nm mounted on a stainless steel rectangular cantilever was used for the bending test. The bending force,  $F_n$ , and the maximum displacement in the z-direction of the beam,  $D$ , were calculated from the following relations,

$$F_n = ((DIF_{init} + DIF_{ex}) / Sensitivity) \times k, \quad (1)$$

$$D = PZT(Z) - DIF_{ex} / Sensitivity, \quad (2)$$

where  $DIF_{init}$  [V] is the initial differential voltage produced by the deflection of the cantilever prior the bending test,  $DIF_{ex}$  [V] is the differential voltage during the test,  $k$  is the stiffness of the cantilever calculated from the Young's modulus of the stainless steel and dimensions of the cantilever,  $PZT(Z)$  [m] is the displacement in the z-direction of PZT actuator settled in AFM and  $Sensitivity$  [V/m] is the ratio of the cantilever's deflection to the displacement of the actuator.

Young's modulus and bending strength  $\sigma_B$  of Si beams were estimated by equations based on the assumption that the beams follow linear elastic theory of an isotropic material. This is due to high specimen length to width and length to thickness ratios and due to the length direction corresponding to the principal stress direction during the test. The Young's modulus and bending strength are expressed as

$$E = \frac{l^3}{192 I} m, \quad (3)$$

$$\sigma_B = \frac{(F_n)_{max} \times e_1}{8 I}, \quad (4)$$

where  $l$  is the beam length,  $I$  is the moment of inertia for the beam cross-section,  $m$  is the gradient of the force - displacement curve,  $(F_n)_{max}$  is the maximum bending force, and  $e_1$  is the vertical distance between the upper surface and the neutral plane.

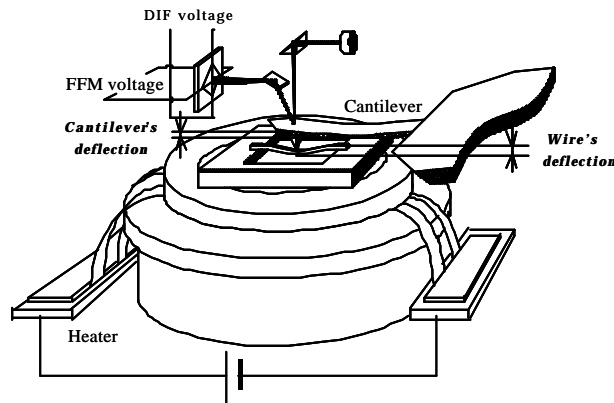


**Figure 3:** AFM bending testing of nano-scale Si beam at intermediate temperatures

## RESULTS AND DISCUSSION

### AFM Bending Test Results

Figures 4 (a) and 4(b) show maximum stress–strain curves of the beams with widths of 200 and 800 nm at each temperature. The stress at the zero strain before bending is due to a pre-load generated when the cantilever was set up on the top of the beam. The Si beam at room temperature fractures in a brittle manner, whereas plastic deformation of Si beams is obtained at intermediate temperatures. Especially, the plastic deformation of the 200 nm-wide beams is induced at even 373 K that is close to room temperature. The figures also show that the plastic strain range obviously increases with decreasing the specimen size and increasing temperature. Comparing the two sized beams above 373 K, the plastic strain range of 200 nm-wide beams is larger than that of 800 nm-wide beams. The specimen size on a nanometer scale has a great influence on the plastic deformation behavior of Si as well as temperature.

The variation of Young's modulus with an increase of temperature is shown in Fig. 5. The Young's modulus decreases with increasing temperature, but does not change with the specimen size. The Young's modulus at room temperature averages 170 GPa, which is comparable to that of micro- or millimeter scale beams [5]. The Young's modulus shows temperature dependency but has no size effect. The temperature dependency is attributed to an increase of the lattice constant of Si due to the thermal atomic vibration, which changes the shape of the interatomic energy curve between Si atoms.

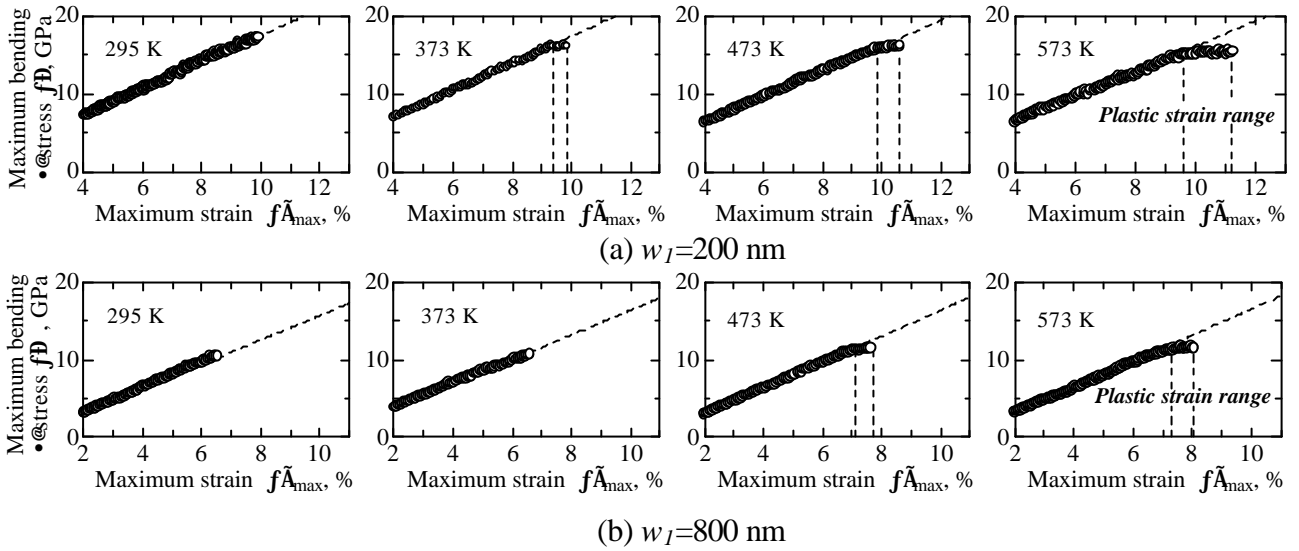


Figure 4: Maximum stress-strain curves in AFM bending testing

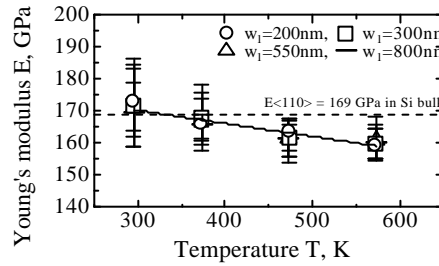


Figure 5: Variation of Young's modulus with increasing temperature

### Weibull Plot

Figure 6 shows Weibull plots of the bending strength. The bending strength of the 200 nm-wide beams ranges from 17.76 to 15.87 GPa, which are approximately 1.5 times larger than that of the 800 nm-wide beams. The beam size therefore has large influence on the bending strength of Si beams. There is also the temperature effect on the bending strength, but it is smaller than the specimen size effect on the bending strength.

Figures 7 correlates the Weibull parameters with the effective volume  $V_E$  and effective surface area  $S_E$  in order to reveal the specimen size and temperature dependency of Weibull parameters [5]. The scale parameter  $b$  decreases with an increase of the effective volume and surface at each temperature. The parameter  $b$  also decreases with increasing the test temperature, which is caused by a reduction of the yield stress at higher temperature. The shape parameter  $m$  is larger in smaller sized beams, but the parameter  $m$  does not have temperature dependency at temperatures applied in the test. The scale parameter  $b$  therefore is affected by the beam size and temperature, but the shape parameter  $m$  is just influenced by the specimen size. In Fig. 8(a), Weibull parameters  $b$  of nano-scale Si beams can be predicted by a function as the following,

$$b = e^{(-3.07T \cdot 10^{-3} + 2.29)} \times S_E^{(5.03T \cdot 10^{-3} - 0.167)}. \quad (5)$$

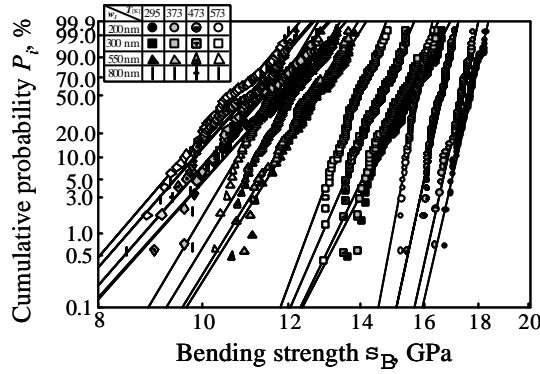


**Figure 6:** Weibull plots of bending strength

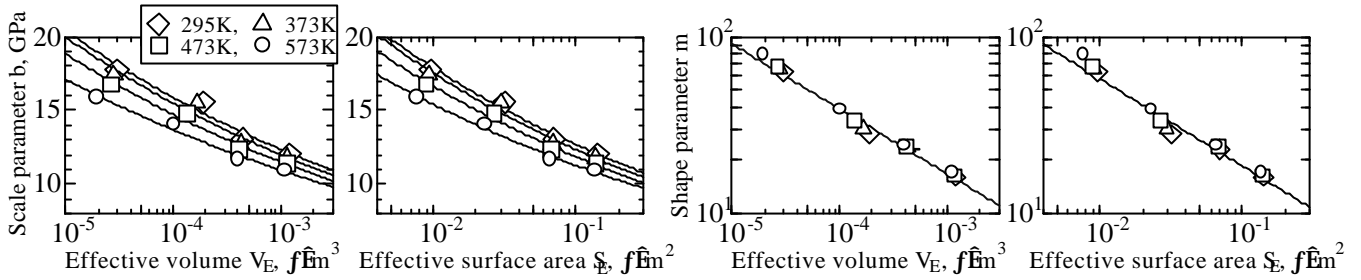


**Figure 7:** Specimen size dependency of Weibull parameters

Figure 8 shows the variation of the critical resolved shear stress  $\tau_c$  for  $1/2 [01\bar{1}] (1\bar{1}\bar{1})$  slip with an increase of temperature, along with results of millimeter sized Si specimens (Casting *et al.* 1981. [6]). Closed plots indicate Si beams wherein the plastic deformation behavior is observed in the beams larger than 60 % of the total number of beams. Half closed and open plots mean Si beams deformed plastically in the beams from 30 to 60 % and less than 30 % of the total number of beams, respectively. The critical resolved shear stress does not only decreases with an increase of the specimen size, but also decreases with an increase of the temperature. So far, it has been reported that plastic deformation in Si on a millimeter scale was not induced below 548 K [6]. However, the plastic flow is obtained at temperatures ranging from 373 K to 573 K in a nanometer-scale specimen. The plastic deformation is then easily induced in smaller sized Si beams on a nano-scale even if test temperature is close to room temperature.

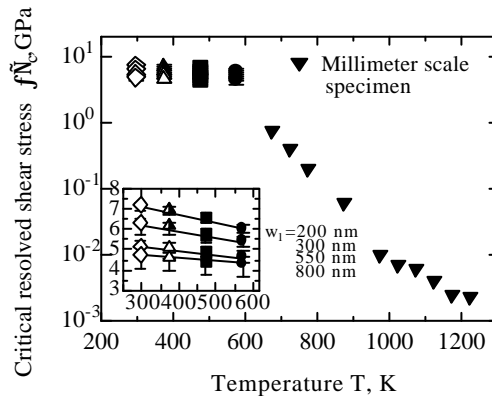


**Figure 8:** Relationship between critical resolved shear stress and temperature

### AFM Observation of Slip Line

For better understanding the specimen size and temperature effects on the plastic deformation behavior, AFM images of the top surface were studied. To examine the slip line produced by dislocations during plastic deformation, the top surface at the end of beam was observed by the AFM as shown in Fig. 9. Several slip lines appear in a smaller sized beam at 373 K, but few slip lines are observed in the 800 nm-wide beams at the temperature. Each slip line is comprised of 1 to 5 nm-high steps as shown in the magnified images. Building up slip lines on an atomic scale, nano-scale Si beams can therefore deform plastically at intermediate temperature. By increasing the deformation temperature the number of slip lines is raised in all of beams. This is caused by an increase of the thermal activation of dislocation.

Figure 10 correlates the slip line density with the effective volume  $V_E$  and surface area  $S_E$ . The slip line density is higher in a smaller sized beam and at higher temperature, which was a similar trend to the beam size and temperature effects on the plastic strain range. The number of slip lines then would have determined the plastic strain range during the deformation. The slip line density in the beam ranges from  $0.5 \times 10^9$  to  $2.5 \times 10^9 \text{ cm}^{-2}$ , which is about 100 times larger than the slip line density in a micrometer scale specimen (Frühaufer *et al.* 1999. [3]). Therefore, the dislocation can easily appear and travel in the nano-scale beam than the micrometer sized specimen. This could be attributed to the effect of an increase of the surface energy with a reduction of the specimen size on the activation energy of dislocation.

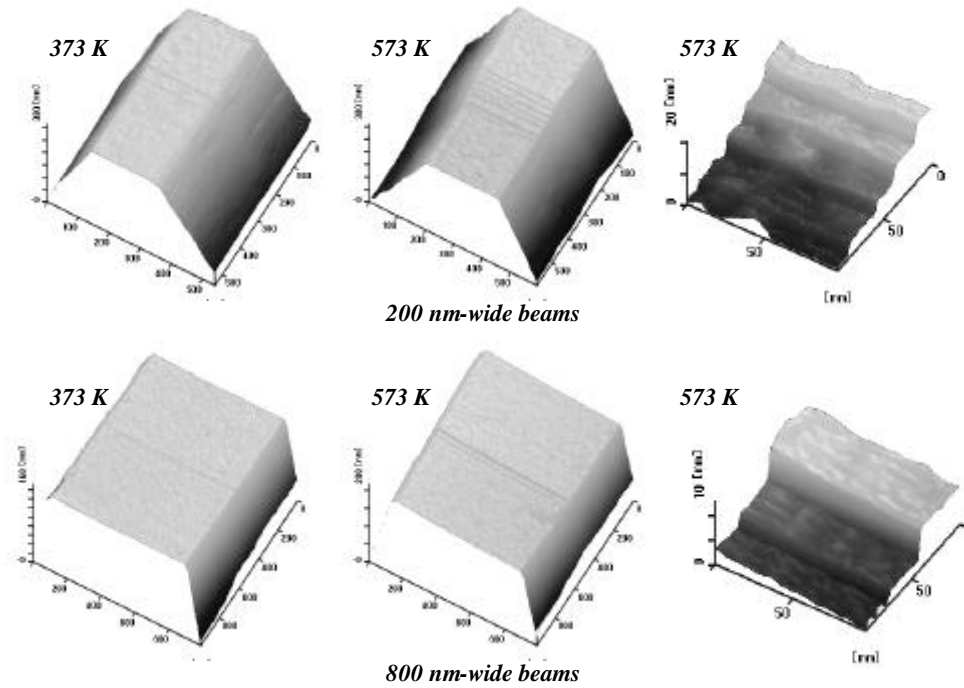


**Figure 9:** AFM images of slip lines at the top surface of Si beams

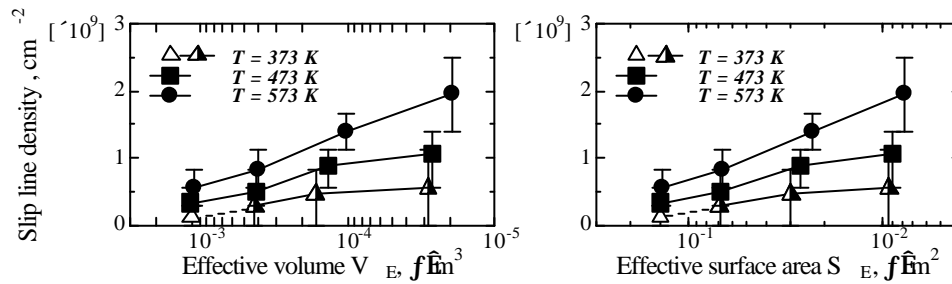


**Figure 10:** Variation of slip line density with a decrease of specimen size

## References

1. Sharpe Jr., W. N., Yuan, Bin and Edwards, R. L. (1997). *Journal of MEMS*, **6**, 3, pp. 193
2. Yi, T. and Kim, C. J. (1999). *Meas. Sci. Technol.*, **10**, pp. 706
3. Frühaufer, J., Gärtner, E. and Jänsch, E. (1999). *Appl. Phys. A*, **68**, 673, pp. 673
4. Hattori, T., Ejiri, Y. and Saito, K. (1994). *J. Vac. Sci. Technol. A*, **12**, 4, pp.2586
5. Namazu, T., Isono, Y. and Tanaka, T. (2000). *Journal of MEMS*, **9**, 4, pp. 450
6. Castaing J. (1981). *Phil. Mag. A*, **44**, 6, pp. 1407